EXPERIMENTAL INVESTIGATION OF GROUTED HELICAL PIERS FOR USE IN FOUNDATION REHABILITATION

Yueying BIAN [1], Tara C. HUTCHINSON[2], Dan WILSON[3], Debra LAEFER[4], Scott BRANDENBERG[5]

ABSTRACT

Building rehabilitation is critical for numerous older urban areas, many of which have inadequate foundations to support new demands. Consequently, development of practical methods to strengthen existing foundations is crucial. In engineering practice, both subsurface grouting and helical piers have been widely used to address these issues by strengthening the foundation. If the solid shaft of a typical helical pier is replaced by a hollow shaft, then helical piers provide the ability to deliver grout. It is hypothesized that these *grouted helical pier systems* (GHPS) could address foundation strengthening needs. This paper presents findings from an exploratory research program where grouting and pier placement tools were developed and tested on the large geotechnical centrifuge at the University of California, Davis. Experimental methods and procedures developed are presented, and observations regarding the formation of grout bulbs under different conditions are analyzed. Physical observation of the test specimens indicates that average grout bulb diameters of 0.6-1.9 times the helix diameter (D_h) are attainable. For similar grout mixes, 20-50% larger grout bulbs can be attained by adding just a modest amount of injection pressure. Future research may use these results to develop load performance data.

Keywords: Grouting, piers, centrifuge models, rehabilitation, deep foundations

[1]Engineer, KPFF Consulting Engineers, Irvine, USA
[2]Associate Professor, Department of Structural Engineering, University of California, San Diego, USA. Corresponding author: tara@ucsd.edu, Phone: +1-858-534-7436, Fax: +1-858-822-2260
[3]Research Faculty, Department of Civil & Environmental Engineering, University of California, Davis, USA.
[4]Director of Conservation Research, School of Architecture, Landscape & Civil Engineering, University College Dublin, Ireland
[5]Assistant Professor, Department of Civil and Environmental Engineering, University of California, Los Angeles, USA.

INTRODUCTION

There are many mid-twentieth century constructed structures in the United States, which are reaching the end of their design life [e.g., American Society of Civil Engineers (ASCE) report card (ASCE, 2005)]. ASCE rated the nation's infrastructure at an overall D (poor) grade and recommended that $1.6 trillion USD should be spent to alleviate potential problems. The situation is similar in many regions of Europe, where population increases have stimulated building expansions.

Due to the historical value of existing structures and strict zoning laws, there are strong motivators favoring rehabilitation of aging structures over demolition. However, old structures are often plagued with potential safety problems. For example, due to degraded material engineering properties, poor or inadequate initial design, or unforeseen load conditions, the foundation of a structure may not meet current building codes. In addition, older structures may undergo structural renovation to accommodate new functionalities, which may add considerably more load demand to the original foundation (Hertlein and Walton, 2000). Additionally, when subjected to natural hazards, such as earthquakes, older foundations may not be sufficiently strong to resist the increased load demands.

In this paper, a foundation rehabilitation technique, termed *grouted helical pier system* (GHPS) is investigated. This technique is a combination of subsurface grouting and helical piers, each of which has been widely used in engineering practice. It is hypothesized that an economical and efficient way to improve strength and stiffness of an existing foundation is through the combined use of helical piers and pressurized grouting. While experimental studies have been conducted on the helical pier itself, e.g. to determine their suitability for uplifting loads [e.g. Prasad and Rao (1996) in clay; Ghaly and Clemence (1998) in sand] their characteristics, when combined with subsurface grouting, have been largely unexplored. Although used commercially (e.g. Chance, 1991; Rupiper, 2003), the application of this technique is still fairly limited, as observed in a recent survey of American members of the Deep Foundation Institute's Helical Pier Committee (Bian et al., 2006). While full-scale tests by Vickars and Clemence (2000) and model tests (Manke, 2004; Manke and Laefer, 2006; Laefer et al., 2007) validate their potential usefulness, additional experiments are needed to understand the characteristics of these systems under a variety of parameters (e.g. installation techniques, grout and soil characteristics, pier characteristics) and under realistic soil stress conditions.

In this work, model centrifuge GHPS testing has been proposed to study the aforementioned issues. Centrifuge tests play an important role in supplementing costly full-scale prototype tests, while filling gaps in understanding the behavior of GHPSs under a wide range of loading conditions. Furthermore,

centrifuge testing allows prototype soil stresses to be modeled appropriately. As a contribution to these efforts, an exploratory experimental program was conducted to first develop suitable in-flight grout and pier installation tools and techniques, and to evaluate characteristics of the achieved grout bulbs. The purpose of this exploratory program was to develop reasonable installation techniques that would support future GHPS-foundation component testing. Variables in the centrifuge experiments included: (i) grout type, (ii) grout installation pressure, (iii) pier embedment and (iv) installation torque.

EXPERIMENTAL SETUP AND CONSTRUCTION

The NEES centrifuge at the University of California, Davis, with an effective radius of 8.5 meters, and available container area of 1.5 m^2 was used for these experiments (NEES@UCDAVIS, 2006). The centrifuge is capable of carrying a five-ton payload to an acceleration of 75-g. All testing presented herein was performed at a centrifugal acceleration of 15 g. A model container with inside dimensions of 1722 mm (length) by 686 mm (width) by 700 mm (height) was used. At 15 g's, this represented a prototype soil area of over 25 m x 10 m and prototype depth of over 10 m, which provided enough space for pier embedment, while minimizing the possibility of any boundary effects. All dimensions presented herein are in prototype units unless stated otherwise (see e.g. Kutter (1992) for a complete description of centrifuge scaling laws).

Schematics of the centrifuge test plan are provided in Fig. 1, and a detailed test matrix is provided in Table 1. The model included 16 helical piers and two plain piers, with a driving system consisting of gear motors; racks and driving block; grout chambers; mac valves, which control the delivery of grout; and an air pressure supply. Each helical pier consisted of a brass shaft with an O.D. of 106 mm, an I.D. of 96 mm, a helix diameter of 381 mm, and a helix pitch of 77 mm. Parameters varied in the centrifuge test plan included the grout type, grout installation pressure, pier embedment, and pier torque (Table 1).

Grout mixes used in the centrifuge tests are presented in Table 2. The grout designed for the centrifuge test was based on results from one-g experiments. During these experiments, the grout mixes demonstrated excellent flowability, relatively long pot life, and high strength (Bian et al., 2006). In addition, grouts were designed with different water/cement (w/c) ratios (0.4-0.6) and additives to improve performance during centrifugal loading. A water reducing agent of between 1-1.5% and between 5-8% silica fume was used to evaluate reduced segregation of the mix during long placement times. Long set time, with minimal segregation, was desirable to allow for adequate time for centrifuge model spin-up. For all mixes, super fine cement and mighty-150 water reducer (both supplied by Nittetsu Cement Company) was used. Grout

and soil conditions were selected to complement and to compare to experimental work previously performed (Manke, 2004; Laefer and Manke, 2006; Laefer et al., 2007).

Model Instrumentation

As the focus of this study was on grout installation and the formation of grout bulbs, most of the experimental data was observational. Therefore, the most important instruments in these experiments were the cameras mounted to monitor images of pier driving and to monitor the grout flow in the transparent tubes. In addition, the photographs, notes, and measurements taken during excavation were invaluable.

In addition to the above instrumentation, these tests provided a unique opportunity to explore the use of imaging techniques to monitor, without excavation, the grout bulb formation and extent. Tomographic imaging provides a method by which shear wave velocity can be extracted before, during, and after grout placement to assist with characterizing the grout dispersion. In these tests, a polar array of bender elements was used to measure shear wave velocity travel times in the region where pier B2 was grouted (Fig. 2). The array was placed at a model-scale diameter of 152 mm to assure the benders would not become encapsulated by an expanding grout bulb (the maximum diameter of the grout bulb was estimated to be less than 90 mm). Travel times were collected at each receiver for shear waves generated at each source before and after grouting to explore the ability of shear wave velocity tomography to image the interior region of the polar array, as discussed later. In addition, two rows of free field benders were placed in the soil (at 254 and 381 mm) to evaluate the soil conditions. Additional details regarding the bender system design and validation may be found in Brandenberg et al. (2006).

Soil Profile and Characterization

Soil used for the centrifuge model was #30 sand obtained locally from White Cap Construction Supply. Fig. 3 shows the grain size distribution curve for this soil. For comparison, the #30 sand, which is obtained from a different vendor and used in the one-g proof-of-concept tests (Bian et al., 2006) is also shown. These two sands have fairly similar grain size distributions. A majority of the sand particles are retained on the 50 sieve, with a small percent of fine aggregates present. From the grain size distribution curve, the Cc and Cu of the sand is 2.32 and 0.79, respectively. According to the Unified Soil Classification System, this type of sand is considered poorly graded. ASTM maximum and minimum density tests (ASTM D 42530-00 and ASTM D 42540-00, respectively), indicate a minimum density of 13.9 kN/m^3 and a maximum density of 16.6 kN/m^3. The sand was placed into the soil container by air pluviation, to obtain a uniform relative density of 80%. After several trials, a relative density of 84% was achieved steadily with the soil unit weight of 16.1kN/m^3.

Model Construction

Unlike the field construction of grouted helical piers, the sequencing of constructing the centrifuge model required placement of the piers and associated below-ground instrumentation at one-g and subsequent grouting in-flight. Although driving the piers in the field will no doubt change the in-situ soil stress conditions, it was deemed necessary to control the placement of the piers (and instrumentation) in the model, by placing them at one-g. Alternatively, it was desirable to grout in-flight, while the soil was subjected to prototype overburden stresses. In addition, applying toque to the piers while grouting in-flight, was conducted for select piers, to study the formation of grout bulb development during mixing. A nominal torque distance of two pier diameters was selected, to minimize complications of driving the entire depth in the centrifuge model. These piers were initially "set" at a pre-defined depth, and subsequently torqued via a drive motor simultaneous with grout delivery. Note that for these "with torque" cases, the piers were subsequently drawn down into the soil, thus mimicking the piers installation process.

Model preparation at one-g involved first placing a lower layer of sand by air pluviation. The bottom set of free-field benders was then laid in the middle of the container. Subsequently, four long piers were located by a string layout and placed in the container. Pluviation was continued to the elevation of the bender circle and the top set of free-field benders. All short piers were then placed in the container and the final pluviation of the upper sand layer was completed. After moving the centrifuge model onto the arm, above-ground instrumentation and the installation/grouting assembly was mounted onto the container edges. The instrumented centrifuge model is depicted in Fig. 4.

EXPERIMENT EXECUTION, RESULTS AND DISCUSSION

Centrifuge Test Execution

Seven spins were performed for this centrifuge test series; complete test series and observations are reported in Bian (2006). Since this pilot study focused on developing techniques, the model was carefully monitored during and after each spin, and modifications were made to the construction techniques and the grout mixture between spins to improve the grout installation and pier draw down. In general, during each spin, three piers were grouted and torqued simultaneously and one pier was grouted without torque.

The grout mix was placed in the chamber as the final step before spin up, to minimize the potential for grout hardening prior to completion of the installation. In the first two spins, grout segregation was observed to occur faster and more severely than expected. Upon examination after spinning, much of the solid portion of the mix was found still in the chamber, while a highly fluid cementitious grout had been

delivered through the pier and into the soil. The super fine cement grout worked well at one-g without obvious segregation after more than two hours (Bian et al. 2006), however, it was unsatisfactory at 15-g. It is postulated that at one-g, the grout mixture has sufficient particulate cohesion to inhibit segregation, a phenomenon mainly due to Brownian motion and one that is slow to develop. However, at 15-g centrifugal acceleration, the centrifugal force overcomes the cohesion. Segregation occurred rapidly as the heavier sand particles were forced out of suspension. To overcome this, several approaches were attempted. Prior to the third spin, as a first attempt, a funnel was attached to the bottom of each chamber and a larger diameter tube was used to mechanically shorten the grout flow time, while helping guide the grout downward towards the pier. Unfortunately, no obvious improvement was observed compared with earlier spin results. In the final spin, Silica fume was added to the grout mix. It was thought that the very fine Silica fume particles (medium particle size: 0.5μm) would fill in the spaces between cement grains (median particle size: 3μm), hence reducing the water content and increasing the cohesion between particles. It was suspected that the addition of Silica fume did provide improvement to the grouting in-flight, however, no substantial improvement was observed in these experiments due to leakage of the tube connections at these pier locations. Consequently, additional testing is needed to quantify the potential for this improvement.

In-Place Soil Characterization

CPT profiling was conducted in the middle of the container, as shown in Fig. 1. Note that the CPT probe was only capable of penetrating into the sand to a prototype depth of 1.6 m, an elevation shallower than the model pier embedment. However, the sand layer was constructed to be very uniform; therefore, one can infer properties at depths based on shallow response. The measured cone resistance versus depth from the CPT is shown in Fig. 5.

To characterize the in-place mechanical properties of the sand in the model, published empirical correlations are used. Cone tip resistance may be correlated with relative density as (Kulhawy and Mayne, 1991):

$$D_r^{\,2} = \left(\frac{1}{Q_F}\right)\left[\frac{(q_c / p_a)}{(\sigma_o' / p_a)^{0.5}}\right] \qquad (1)$$

where, p_a = atmospheric pressure, σ'_o = vertical effective stress, q_c = cone tip resistance, Q_F = an empirical constant. As suggested in Kulhawy and Mayne (1991), Q_F is selected as 305 for sands with medium compressibility. To use Equation 1, and in light of the shallow penetration of the CPT, the deepest region of measured cone resistance is considered, resulting in a the relative density (Dr) at 1.6 m estimated as 80%, which is consistent with the expected D_r of 84%.

Similarly, an estimate of the in-place strength of the sand may be determined using the relation by Robertson and Campanella (1983):

$$\phi' = \tan^{-1}[0.1 + 0.38 * \log(q_c / \sigma'_0)] \quad (2)$$

Based on Equation 2, the calculated friction angle ranged from 42˚ to 46˚ between the depths of 1.4 m and 1.6 m. For an estimated relative density of 80%, and a friction angle range of between 42˚ and 46˚, the in-place sand for the model may be characterized as dense sand (Meyerhof, 1956).

In-Place Grout Characteristics

After placing the premixed grout into each chamber before spinning, the remaining grout was cast into 50 mm diameter cylinders. Compressive strength tests were performed on the same day of the spin, and 18-24 days post-placement. The range of compressive strengths at 18-24 days was 23.7-40.7 MPa, with a mean of 30 MPa, and standard deviation of 7.4 MPa. It is noted that these strengths are slightly high for typical grout and more comparable to conventional concrete mixes. This high strength may be attributed to the ultra-fine cement and low w/c ratio, which is slightly lower than most field placed grout. However, as noted previously, these mixes performed well at one-g using the pier-sand combinations planned for the centrifuge tests. Grout C and D, with the Silica fume addition, and lowest w/c ratio (0.40) had the highest strengths, while grout B, with the largest w/c (0.6) had the lowest strengths.

Experimental Results

Using the above described grout mixes, grout bulbs were generated in-flight and characterized through post-experiment excavation. In addition, select regions of the soil were imaged using bender element arrays. Tomographic imaging has shown promise for quality assessment of grouted piers in the field, and centrifuge studies provide an opportunity to explore such methods.

Tomographic Imaging

Tomographic images of the interior region of the polar array of bender elements placed around pier B2 (see Fig. 2b) were constructed from shear wave travel time measurements collected before and after grouting, while the centrifuge spun at 15-g. The bender element system was recently developed prior to the centrifuge test (Brandenberg et al. 2006), and the test provided an opportunity to (i) evaluate the ability of the bender element system to accurately measure shear wave velocities while the model spun on the centrifuge, and (ii) explore tomographic imaging techniques to "see" the grout bulb non-invasively. Travel times were picked from the recorded signals, the region between the bender elements was

discretized into pixels, and the unknown values of shear wave velocity of the pixels were obtained by tomographic inversion following methods described by Santamarina and Fratta (2005). The resulting tomograms are presented in Fig. 6a. The tomograms showed that the shear wave velocity of the soil was uniformly about 210 m/s before grouting, which is reasonable for normally-consolidated dense sand under the imposed overburden stresses (Arulnathan et al. 2000). Furthermore, the 0.57m (prototype) diameter grout bulb (Fig. 5b) near the center of the array after grouting was clearly identifiable after grouting.

While the bender element system was able to measure the shear wave velocity of the sand and identify the presence of the grout bulb by tomographic inversion, a number of limitations were also identified. The shear wave velocity of the grout predicted by tomographic inversion (600 m/s) is lower than the expected values (approximately 1570-1800 m/s). The experimental setup is unable to accurately resolve the shear wave velocity of the grout bulb, because the error in the inversion is not very sensitive to changes in shear wave velocity of the grout (e.g., increasing the shear wave velocity of the center pixels to 1200 m/s has little effect on the difference between measured and predicted travel times). Furthermore, the pixel sizes are large compared with the size of the grout bulb, hence the shape and position of the bulb could not be accurately resolved. Both of these limitations can potentially be resolved by different sensor configurations, and better methods of signal interpretation. Despite the limitations, further verification of the tomographic imaging with post-experiment inspection (as will be shown below) demonstrates how tomographic imaging, currently in its infancy in its application to centrifuge modeling, shows promise for accurate non-invasive quality assessment of subsurface construction.

Post-Experiment Physical Inspection

Ten days following the final spin, after the grout was thoroughly hardened, the model container was physically excavated, and each grouted helical pier was carefully removed from the container. Results of the 15 excavated piers are summarized in Table 3, where the geometric notations used are depicted in Fig. 7. Note that dimensions listed in Table 3 are prototype dimensions. Of the 15 piers grouted, 40% (six) exhibited poor performance during installation. For example, four helix-pier connections failed during torquing (i. e., the pier did not draw itself into the soil with rotation), while two piers suffered from grout leakage during installation due to a poor seal at the funnel-chamber connection. Failure of the pier to be drawn down during applied torque, which occurred in the first few spins, was observed during spinning, via the on-board video system. This was solved in subsequent tests by providing a manual application of torque to the pier, effectively seating the pier in the sand prior to spin-up. Despite these failures, much information was obtained from these as well as the successfully grouted piers.

Photographs of the excavated piers and grout bulbs are shown in Fig. 8. In general, the soil-grout bulbs can be characterized by a larger, spherical region surrounding the helix, at the point of grout export (Fig. 7), and a region of thinner, 'finger-like' extensions, well below the bottom of the pier. The spherical region of the grout bulb core is consistent with physical observations of 'tear-drop' shaped grout bulbs, which developed during centrifuge experiments of Nichols and Goodings (2000). The 'finger-like' extensions observed herein tended to extend 2-4 times longer than length of the spherical main body surrounding the helix. The physical size of the 'finger-like' extensions was measured and recorded (L_f) as noted in Table 3. The range of L_f was between 38 and 133 cm (prototype), which was generally between 1/3 to 1/2 of the total grout bulb length. The total additional weight of the grout bulb placed at each pier is also estimated, including the finger extensions, to be between 341 - 721 kg, excluding those below 100 kg, where physical problems with installation were observed.

The maximum grout bulb diameter D_{max} ranged between 14 and 81 cm. The low values (D_{max} = 14 and 19 cm) occurred in those cases where physical problems occurred with the installation. The range of D_{max} was approximately 0.4 – 2.1 times the helix diameter. Excluding the data from spin six (where tube leakage was observed), the range of D_{max} was 0.9 – 2.1 times the helix diameter. Despite the slight differences in installation, this is fairly consistent with observations by Manke (2004) during $1/8^{th}$ scale 1-g tests, who noted grout bulbs approximately 0.9-1.2 times the helix diameter, with an average of 1.0 and standard deviation of 0.1. The length of the major grout bulb (less the finger extensions, noted as L_b) ranged from 67-191 cm (excluding those with physical installation problems). This range generally matched or exceeded the length region over which the target simultaneous grouting and torquing of the piers was conducted (76 cm target draw down depth).

Parametric Study and Discussion

Considering the variables used in the test matrix; embedment depth (L_e), injection pressure (P_i), grout type and the use of rotation; a parametric study is performed to understand their relative impact on the resulting grout bulbs. In the analysis, the average diameter (D_{ave}) is used to represent the size of the grout bulb, where D_{ave} is taken as $(D_{max}+D_{min})/L_b$, and the weight (W_{GB}) is used to provide an indication of the overall in-place size. In the following Figures, the diameter is normalized as D_{ave}/D_h, where D_h is the helix diameter, and the weight is normalized as W_p/W_{min}, where W_{min} is the minimum grout bulb weight obtained.

In Fig. 9a, four scatter plots of L_e versus D_{ave}/D_h are presented, which correspond to four construction combinations: use of (i) Grout A (see Table 2) with rotation, (ii) Grout B (see Table 2) with rotation, (iii)

Grout A without rotation, and (iv) Grout B without rotation. Fig. 9b presents similar data as scatter plots of L_e versus W_p/W_{min}. Results in Fig. 9 indicate that the grout bulb diameter D_{ave} ranged between 0.6-1.9 that of the helix diameter, with an average of 1.3 and standard deviation of 0.4, under the same soil and grout conditions. In all embedment cases, Grout A bulbs yielded a larger D_{ave}/D_h value than Grout B bulbs, under both rotation and no-rotation conditions. This may be attributed to the lower w/c ratio of Grout A (0.45), as compared with Grout B (0.60), which also had a consistently higher compressive strength (approximately, 30-40% greater than Grout B). This diameter increase for Grout B, when the piers were rotated (50% increase at 3.8 m depth), was more obvious than that of the non-rotation situation (32% increase at 3.8 m depth). Nonetheless, in all cases, the use of simultaneous rotation and grouting increased the average grout bulb diameter. This is consistent with expectations, that the helix will force the grout mixture outwards into the soil, further than it could penetrate on its own. Furthermore, for greater embedment depths, the grout permeated to a larger diameter. Grout B bulbs at 5.7m (L_e = 5.7m) resulted in about a 42% larger diameter than Grout B bulbs at 3.8 m (L_e = 3.8m). This may be attributed to the larger pressure head at greater depths, helping push the grout into the dry soil.

Similar trends may be observed when considering the effects on the final grout bulb weight, as normalized by the minimum grout bulb size, W_p/W_{min}. As observed in Fig. 9b. The increase in the in-situ bulb weight was sensitive to the depth of embedment L_e, and was larger for deeper piers. The effect of rotation was also more pronounced. Including rotation resulted in a factor of 10-12 increase in the weight ratio W_p/W_{min}.

Figures 10a and b are used to study the grout installation performance as a function of the grout injection pressure at the grout exit hole. In these figures, the grout injection pressure at the grout exit hole (P_x) is defined as the sum of the overburden pressure at the exit hole and the injection pressure, $\gamma L_e + P_i$, where γ is the bulk unit weight of the grout mixture, L_e is the embedment depth, and P_i is the added air pressure. In Figures 10a and b, the three values of P_x, are the result of: (i) 3.8m embedment depth (0.16MPa), (ii) 3.8m embedment depth plus 0.171 MPa air pressure (0.19MPa) and (iii) 5.7m embedment depth (0.23 MPa). Generally, it is observed from Figure 10a and b that for the same type of grout, the grout bulbs under higher injection pressures are larger. This is consistent with observations by others regarding the sensitivity of grout bulb size due to overburden pressure (e.g. Nichols and Goodings, 2000). In general, the pier rotation also greatly increased the grout permeation, with one exception. This case was the outlier at D_{ave}/D_h = 2.0 and W_p/W_{min} = 25.4, which correspond to the case of Grout B installed without rotation and an injection pressure of 0.23MPa. This case can be attributed to the excessively high injection pressure, which overcame the overburden pressure. Therefore, the grout actually intruded (fractured) the

sand mass instead of permeating into the sand voids, resulting in an abnormally large grout bulb. It should be noted that fracturing the soil during grout applications can result in unpredictable and sometimes unfortunate consequences.

From the above parametric study, it is concluded that, first Grout A with a lower w/c ratio generated larger grout bulbs than Grout B, when placed under the same installation conditions, i.e. the embedment depth and the use of rotation. Secondly, pier rotation, greater embedment depths and higher injection pressure all positively improved grout permeation performance, resulting in larger grout bulbs.

Grout Fingering

Grout fingering was observed in the final grout bulbs as shown in Fig. 7 and 8. Here, "fingering" refers to the infiltration of grout mix through the sand in columns of flow. This phenomenon was not observed in the one-g tests and thus can be attributed to the increased centrifugal field applied to the model. This type of fingering is caused by unstable flow during infiltration into unsaturated homogeneous porous media (Selker et al., 1992; Wang, et al., 2004). Note that pier rotation, deeper embedment depth and higher injection pressure all increased the lengths of the observed fingering extensions.

A number of theoretical and experimental studies have been conducted to explain the occurrence of fluid instability under different conditions. One reasonable explanation was proposed by Geiger and Durnford (2000). In their work, an experimental study on the infiltration in homogeneous sands was conducted, and they concluded that a critical flux value exists for fine sands. The authors noted that below this flux value, stable flow occurred, and above this flux, flow was unstable, which resulted in a fingering phenomenon. In the study presented herein, although the pore geometry and permeability remain the same at higher g-levels as that at the 1-g level (Culligan et al., 1997), the grout fluid velocity and the seepage flux are increased by 15 times at 15-g. When the flux value of the grout fluid is larger than the critical flux value of the sand, the grout flow may become unstable.

Assuming the unstable flow phenomenon above, one may estimate the finger's width theoretically using the approximation for finger extension width (w) proposed by Parlange and Hill (1976):

$$w = \frac{\pi * S_F^{\,2}}{\Delta\theta(K_F - u\Delta\theta)} \tag{3}$$

where q_s = the flux through the system, q_F = the average finger flux, u = the velocity of the unperturbed flat front, S_F = sorptivity, $\Delta\theta = \theta_F - \theta_0$, θ_F is assumed to be equal to the effective saturated moisture content of the soil. The water content change, $\Delta\theta$, does not vary between model and prototype; therefore, neither

will the sorptivity (Culligan et al., 1997). For the dense #30 sand used herein, the sorptivity is estimated as 0.72 mm/s^{-2}, therefore, $S_F^2 = 5.2x10^{-3}$ cm^2/s. Note that typically infiltration experiments are carried out to determine the S_F, K_F and $\Delta\theta$. Using the factors estimated from the literature, K_F = 0.2 cm/s, $\Delta\theta$ = 1, and u = 0.197 cm/s. Therefore, Equation 3 results in w ≈ 5.5 cm in prototype. After excavation, grout bulbs were observed to have finger extension widths approximately 0.4 cm, which, if multiplied by N=15 (g), results in 6 cm in prototype. This observation is in agreement with the theoretical estimates. The observation of fingering phenomenon in this test is an important consideration in interpreting centrifuge model performance and evaluating mechanisms, particularly how they can be applied to field conditions.

CONCLUSIONS

One promising technique for rehabilitating existing foundations, which has seen little attention in the literature, is the use of the *grouted helical pier system* (GHPS). This paper focuses on developing centrifuge testing tools for the study of the GHPS (or similar grouting-based rehabilitation systems). In-flight grouting and in-flight pier installation were successfully performed simultaneously in the centrifuge testing. In the analysis of centrifuge test results, a parametric study of the observations regarding the developed grout bulbs under different conditions is performed. Experimental advancements are summarized as follows:

- To address the small-scale model requirements on the centrifuge, grout mixes were designed with microfine cement. These mixes proved suitable, by providing a sufficiently long pot life, adequate fluidity, and strength. This allowed proper placement and successful grout transfer through the small model pier and permeation through the soil. However, grout segregation was also observed at 15-g due to the inevitable 15-g inertia force. Silica fume showed promise to alleviate the segregation, however, further testing is needed.
- The soil in the centrifuge model was instrumented with an array of bender elements placed around the grout bulb location, and the bulb was non-invasively imaged using travel-time tomography. The tomograms clearly indicated the presence of the grout bulb. This proof-of-concept study shows promise in the future for using shear wave velocity measurements to non-invasively image subsurface construction.
- *Parametric analysis* of the grout permeation performance as observed through physical post-experiment excavation reveals that (i) grout bulb diameters ranged between 0.6 and 1.9 times that of the helix diameter (D_h), averaging 1.3 times D_h, (ii) grout with a lower w/c ratio generated larger grout bulbs under comparable installation conditions, (iii) the increase in in-situ bulb size was sensitive to the depth of embedment and was larger for the deeper piers, (iv) by rotating the pier during grout installation, the generated grout bulbs' average diameter increased

approximately 60-100%, and (v) for the same type of grout, observed grout bulbs under higher injection pressures are larger. For example, the addition of 0.7 MPa (10psi) air pressure can provide a 20-50% increase in grout bulb diameter and a 10 – 45% increase in grout bulb weight.

- A simple study of the *fingering phenomena* observed due to the increased g-field applied to the model indicates that grout with a lower w/c ratio generated longer fingering extensions. While this might be counterintuitive, as one might expect that a more fluid mix would have a greater tendency to be pushed through the soil and flow with the inertial load, the lower w/c ratio likely had a greater amount of heavier cement particles in suspension, and this could increase the likelihood for fingering. Furthermore, pier rotation, deeper embedment depth and higher injection pressure all increased the lengths of the observed fingering extensions. The finger extension widths could be reasonably estimated using theoretical methods.

AKNOWLEDGEMENTS

This work was supported by the Civil and Mechanical Systems Division of the U.S. National Science Foundation (NSF) [CMS-0513972], where Dr. Richard Fragaszy is the program director. NEES Operations and Maintenance funding supports the operation of the centrifuge at UC Davis (NSF Award CMS-0402490). Grouted materials were donated by Surecrete, Inc. and DeNeef Construction Chemicals. Assistance was provided by UC Davis centrifuge staff and particular Chad Justice and Lars Pederson. Helpful suggestions and technical input were provided by Dean White of Concrete Technologies and Russell Lindsey of Precision Pier USA, Inc. Opinions, findings, and conclusions in this paper are those of the authors, and do not necessarily reflect those of the sponsoring organization.

REFERENCES

AB Chance Co. (1991). "Foundation and underpinning system." BuyLine 1386, A.B. Chance Co., Centralia, MO. (http://www.abchance.com/). Retrieved October, 2007.

Arulnathan, R., Boulanger, R. W., Kutter, B. L., and Sluis, B. (2000). "New tool for shear wave velocity measurements in model tests." *Geotechnical Testing Journal*, GTJODJ, ASTM, 23(4): 444-453.

ASCE, American Society of Civil Engineers (2005), *ASCE report card for America's Infrastructure*. from: http://www.asce.org/reportcard/2005/. Retrieved October, 2007.

Bian, Y. (2006). *Development and Testing of Centrifuge Tools for Use in Grouted Helical Pier based Foundation Rehabilitation Studies*, Masters Thesis, University of California, Irvine.

Bian, Y, Hutchinson, TC, Wilson, D, and Laefer, D. (2006). Grouted Helical Piers for Use in Foundation Rehabilitation: Considerations for Small-Scale Centrifuge Testing. *In the Proceedings of the International Conference on Re-use of Foundations for Urban Sites* (RuFUS 2006), BRE, Garston, UK, 14–15 June.

Brandenberg, S.J., Choi, S., Kutter, B.L., Wilson, D.W., and Santamarina, J.C., (2006). "A bender element system for measuring shear wave velocities in centrifuge models", *6th International Conference on Physical Modeling in Geotechnics*, Hong Kong University of Science and Technology, Hong Kong, 1:165-170.

Culligan, P.J., Barry, D.A., and Parlange, J.Y. (1997). "Scaling unstable infiltration in the vadose zone." *Canadian Geotechnical Journal*, 34: 466-470, 1997.

Ghaly, A.M. and Clemence, S.P. (1998). Pullout performance of inclined helical screw anchors in sand. *ASCE Journal of Geotechnical and Geoenvironmental Engineering*. 124(7): 617-627.

Geiger, S.L., and Durnford, D.S. (2000). "Infiltration in homogeneous sands and a mechanistic model of unstable flow." *Soil Science Society of America Journal*, 64: 460–469.

Hertlein, B.H. and Walton, W.H. (2000). "Assessment and reuse of old foundations." *Transport Research Record*, No. 1736: 49-54.

Kulhawy, F.H. and Mayne, P.W. (1990). *Manual on estimating soil properties for foundation design*. Report EL-6800, Electric Power Research Inst., Palo Alto, 306 pp.

Kutter, B.L. (1992). Dynamic centrifuge modeling of geotechnical structures. *Transportation Research Record*, No. 1336, pp. 24-30.

Laefer, D., Manke, J., Tucker, J., and Batten, Y. (2007). "Challenges to Model-Scale Testing for Composite Deep Foundations and Existing Foundation Enhancement" Geo-Denver 2007: New Peaks in Geotechnics, ASCE Spec. Geotechnical Pub. 158 Contemporary Issues in Deep Foundations. (ed. Olsen, H.W.) p. 1-10.

Laefer, D.F. and Manke, J.P. (2006). "Small-scaled Testing of Rehabilitated Pile Groups." *Int'l Conf. on Re-use of Foundations for Urban Sites RuFUS*. 17-18 October 2006 BRE, Watford, UK.

Manke, J.P. (2004). "Assessment of superposition as a design framework for the combined effects of soil improvement and foundation remediation." *Master's Thesis, North Carolina State University*, 221 pp.

Meyerhof, G.G. (1956). "Penetration tests and bearing capacity of cohesionless soils." *Journal of the Soil Mechanics and Foundation Division, ASCE*, 82(SM1): 1-19.

NEES@UCDAVIS, Retrieved May, 2006, from: http://nees.ucdavis.edu/.

Nichols, S. C. and Goodings, D. J. (2000). "Physical model testing of compaction grouting in cohesionless soil." *ASCE Journal of Geotech. and Geoenvir. Engrg.*, 126(9): 848-852

Parlange J.Y. and Hill D.E. (1976). "Theoretical analysis of wetting front instability in soils." *Soil Science*, 122(4):236-239.

Prasad, Y.N. and Rao J.S.N. (1996). Lateral capacity of helical piles in clays. *ASCE Journal of Geotechnical and Geoenvironmental Engineering*. 122(11): 938-941.

Robertson, P.K. and Campanella, R.G. (1983). "Interpretation of cone penetration tests. Part I: Sand." *Canadian Geotechnical Journal*, 20: 718-733.

Rupiper, S. (2003). *Helice pier coupling system used for soil stabilization*. US Patent No. 941920, Patentstorm: http://www.patentstorm.us/patents/6615554-description.html. Retrieved October, 2007.

Selker, J, Leclerq, P, Parlange, JY, and Steenhuis, T.S. (1992). "Fingering flow into two dimensions, 1. Measurement of metric potential." *Water Resources Research*, 28(9): 2513-2512.

Vickars, R.A. and Clemence, S.P. (2000). "Performance of helical piles with grouted shafts." *New Technological and Design Development in Deep Foundations*, N.D. Dennis Jr., R. Castelli and M.W. O'Neill, editors, Geotechnical Special Publication No. 100, American Society of Civil Engineers, 327-341.

Wang, Z., Jury, W.A., Tuli, A. and Kim, D.J. (2004). "Unstable flow during redistribution: controlling factors and practical implications." *Soil Science Society of America Journal*, 3: 549–559.

List of Tables

Table 1. Centrifuge Test Matrix.

Pier Location	Helix	Motor rotation @ 5rpm	Embedment depth[1]		Grout Mix				Air Pressure[2] (0.17 MPa)
			3.8m (256mm)	5.7m (381mm)	A	B	C	D	
A1, A2	√	√	√		√				
A3	√	√		√	√				
B1, B2	√	√	√			√			
B3, B4	√	√	√			√			√
B5, B6	√	√		√		√			
C1	√		√		√				
D1	√		√			√			
D2	√		√			√			√
E[3]			√						
F[3]	√		√						
G1	√	√	√				√		
G2	√	√	√				√		√
G3	√	√		√				√	

1. Prototype and model scale embedment depths are both listed, with model scale in parenthesis.
2. Except for marked pier locations, grout is installed under atmospheric pressure.
3. Pier E & F are instrumented with strain gauges for loading test only, no grout installation is performed at these two locations.

Table 2. Grout mix summary (percentages by weight of cement).

Grout Mix Type	Water/Cement Ratio (w/c)	Silica Fume	Water Reducer
A	0.45	0%	1.5%
B	0.60	0%	1.0%
C	0.40	5%	1.5%
D	0.40	8%	1.5%

Table 3. Centrifuge test results for grout installation (prototype units).[1]

	Pier No.[2]	L_e (m)	P_i [2] (MPa)	P_x (MPa)	Grout Type[3]	Helix Observation	W_g (kg)	Observation after Excavation[4] (cm)						Possible Explanation
								D_{max}	D_{min}	L_m	L_b	L_f	L	
1st Spin	A1	3.8	0.101	0.16	A	helix failed	0	0	0	0	0	0	0	Helix failed & tube leaked.
	A2	3.8	0.101	0.16	A	embedded in grout	570.7	71	48	24	76	130	206	
	A3	5.7	0.101	0.19	A	embedded in grout	587.9	76	52	10	76	133	210	
2nd Spin	B1	3.8	0.101	0.16	B	embedded in grout	341.2	46	38	38	126	122	248	
	B2	3.8	0.101	0.16	B	embedded in grout	402.3	48	29	10	191	84	274	
	B3	3.8	0.171	0.23	B	helix failed	0	0	0	0	0	0	0	Helix failed.
3rd Spin	B4	3.8	0.171	0.23	B	embedded in grout	559.2	69	45	14	110	69	179	
	B5	5.7	0.101	0.19	B	bulb below helix	548.8	67	48	0	69	122	191	
	B6	5.7	0.101	0.19	B	helix failed	0	0	0	0	0	0	0	Helix failed.
1st Spin	C1(*)	3.8	0.101	0.16	A	outside the bulb	47.3	33	29	0	19	38	57	
2nd Spin	D1(*)	3.8	0.171	0.23	B	embedded in grout	721.6	81	67	10	76	122	198	
3rd Spin	D2(*)	3.8	0.101	0.16	B	outside the bulb	28.4	29	19	0	19	38	57	
6th Spin	G1	3.8	0.101	0.16	C	bulb below helix	58.1	14	10	0	30	0	30	Bottom funnel leaked.
	G2	3.8	0.171	0.30	C	helix failed	0.0	0	0	0	0	0	0	Helix failed.
	G3	5.7	0.101	0.19	D	bulb below helix	81.3	19	11	0	38	0	38	Bottom funnel leaked.

[1] L_e = prototype embedment depth; P_i = grout inject pressure; $P_x = \gamma L_e + P_i$ = total pressure at grout exit hole (γ = soil unit weight: 16.1kN/m^3) W_g = prototype grout bulb weight. All other notations are shown in Fig. 7

[2] All piers torqued at target 5 rpm, those noted with (*) were installed grout without rotation

[3] Table 2 provides the grout mix summary

[4] The embedment depth, grout bulb weight and grout bulb dimensions are all in prototype units

List of Figures

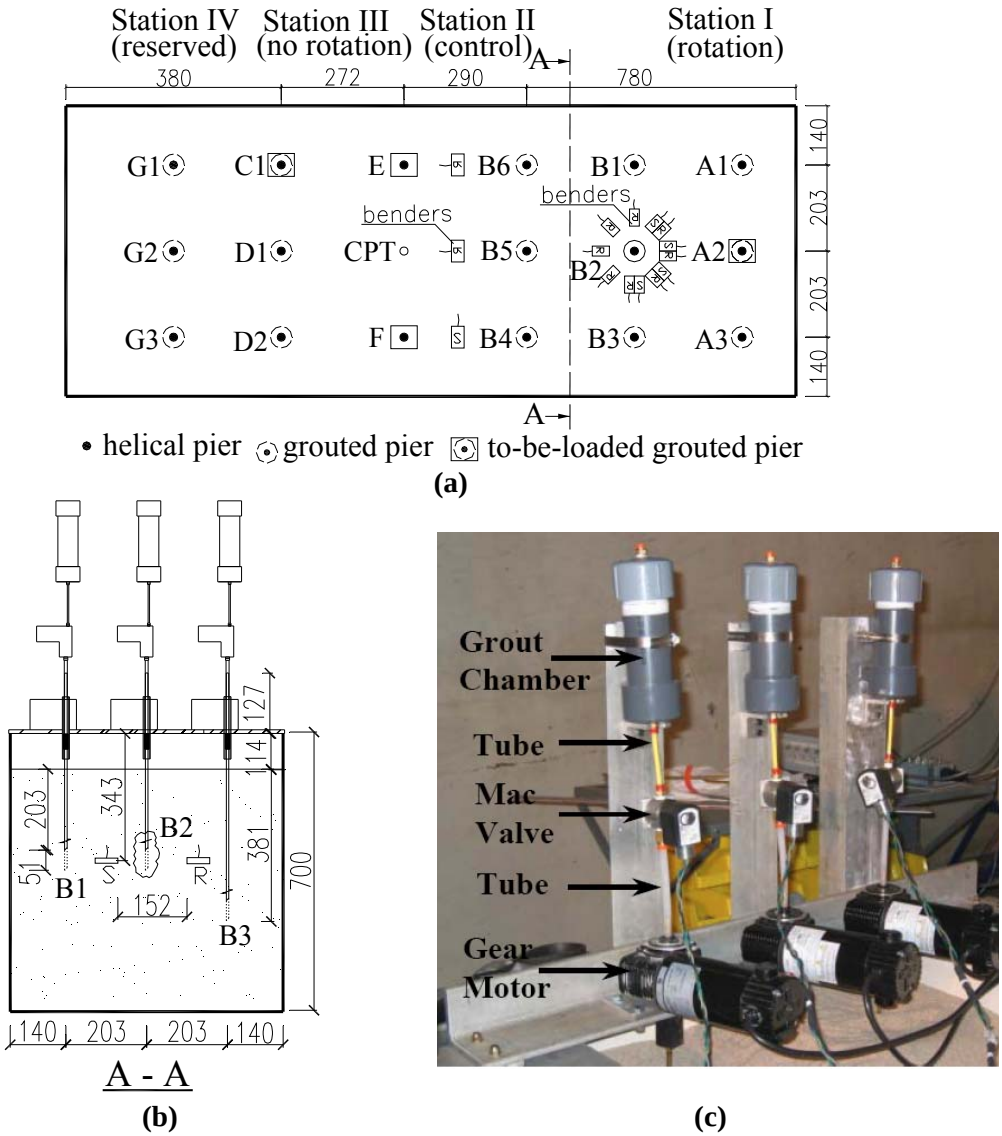

Fig. 1. Centrifuge test layout: (a) plan view, (b) section view, and (c) elevation photo of model pier installation and grouting assembly (units in mm, model scale).

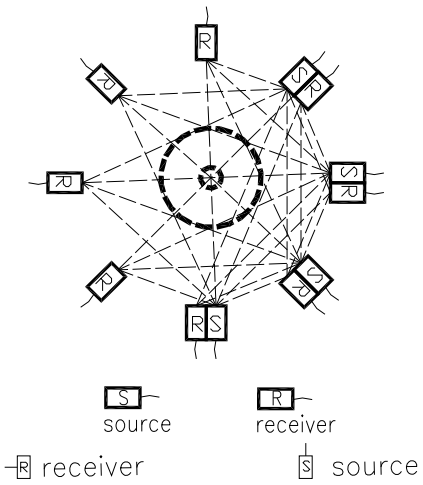

(a)

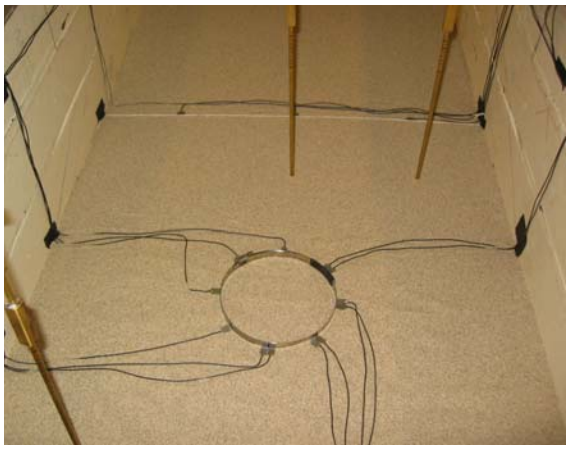

(b)

Fig. 2. (a) Bender element ray path traces and (b) photograph of benders in place (Note: the ring is shown for placement of benders only, and was removed prior to testing).

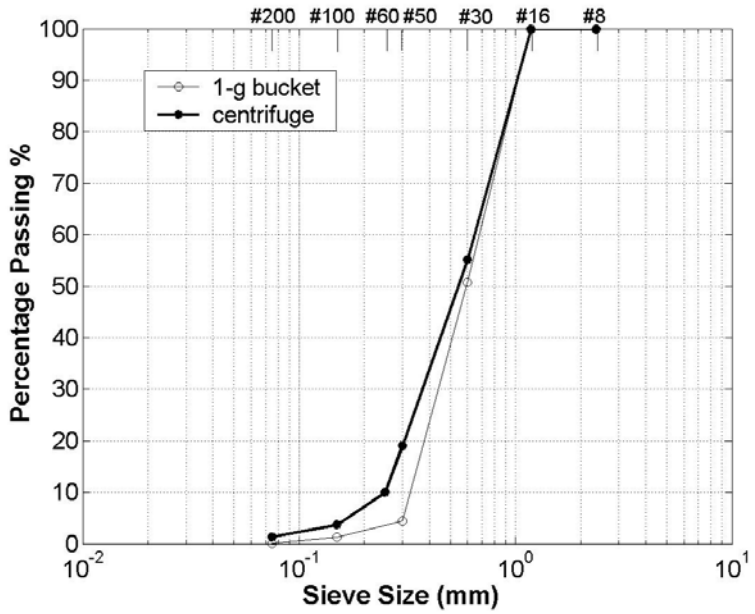

Fig. 3. Grain size distribution curve for #30 silica sand used in one-g bucket (proof) tests (Bian et al. 2006) and in centrifuge tests.

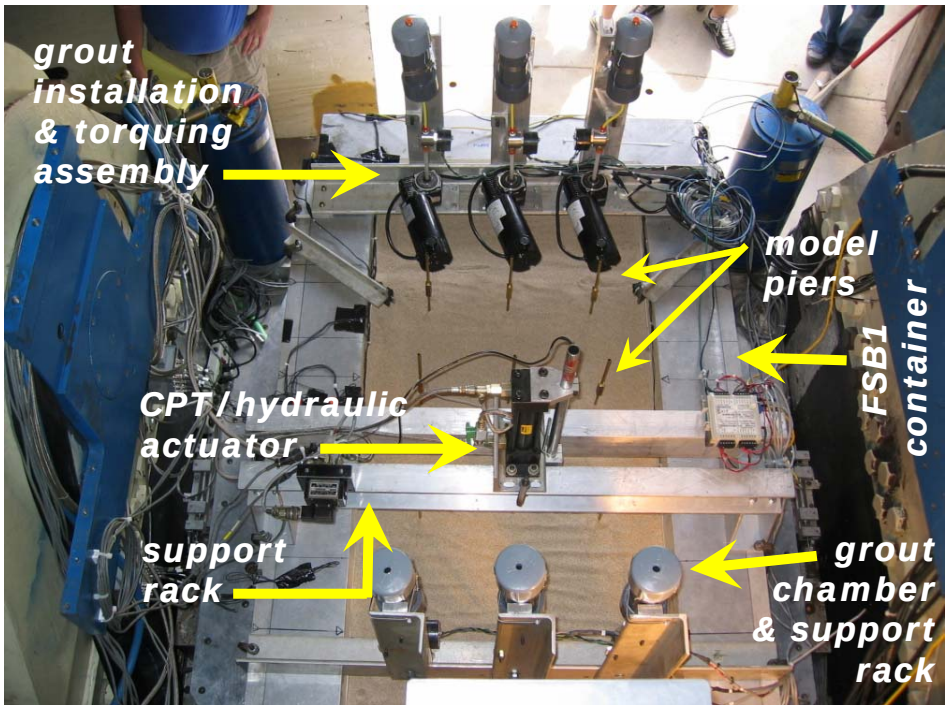

Fig. 4. Model on centrifuge arm.

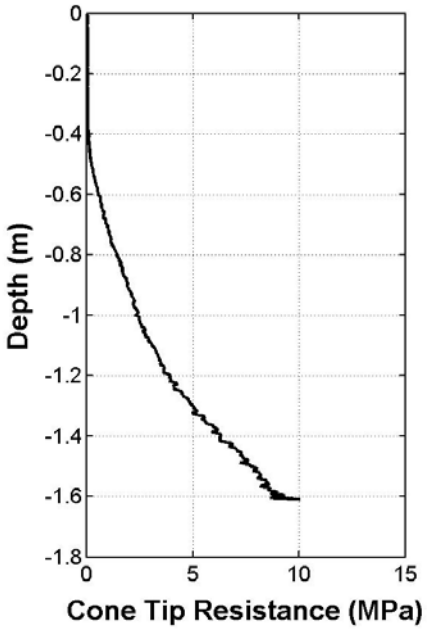

Fig. 5. CPT profile.

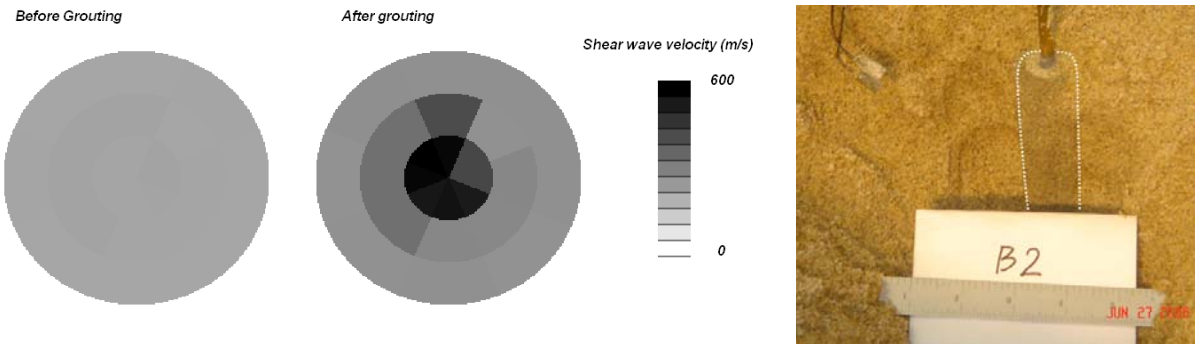

(a) **(b)**

Fig. 6. (a) Shear wave velocity tomograms depicting shear wave velocity profiles before and after grouting (b) photograph of observed grout bulb at location B2.

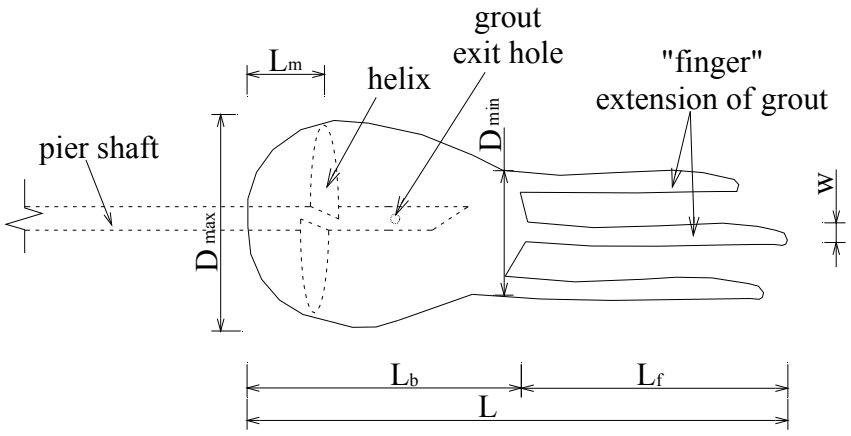

Fig. 7. Dimensional analysis of grout bulbs.

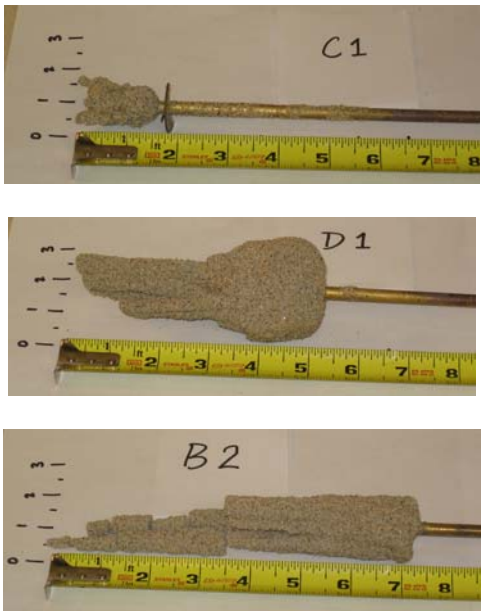

Fig. 8. Photographs of excavated grouted piers.

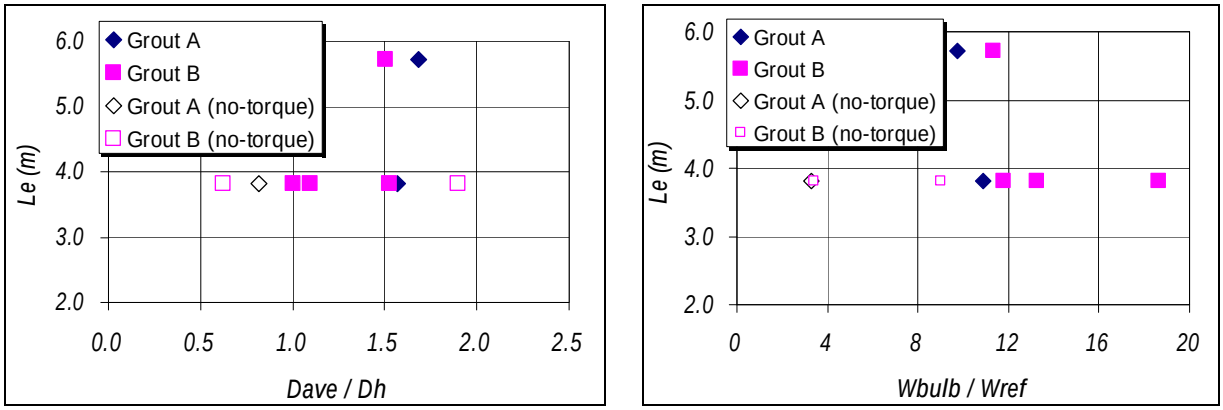

(a) **(b)**

Fig. 9. (a) Normalized grout bulb diameter and (b) normalized grout bulb weight versus embedment depth.

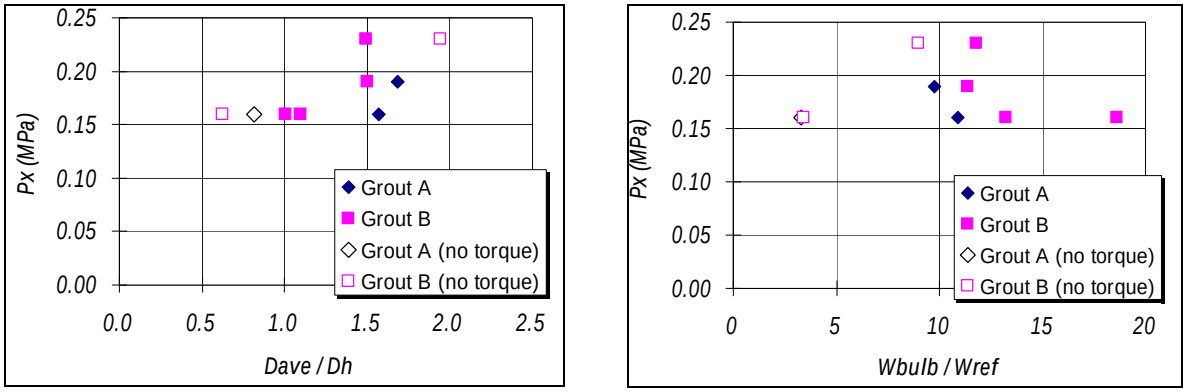

(a) **(b)**

Fig. 10. (a) Normalized grout bulb diameter and (b) normalized grout bulb weight versus injection pressure.